Pure appl. geophys. 152 (1998) 329–348
0033–4553/98/020329–20 $ 1.50 + 0.20/0

Pure and Applied Geophysics

3-D *P*-wave Velocity Structure in Western Greece Determined from Tomography Using Earthquake Data Recorded at the University of Patras Seismic Network (PATNET)

N. S. MELIS[1,2] and G.-A. TSELENTIS[1]

Abstract—The 3-D *P*-wave velocity structure of the upper crust in the region of western Greece is investigated by inversion of about 1500 residuals of *P*-wave arrival times from local earthquake data recorded in the year 1996 by the newly established University of Patras Seismic Network (PATNET). The resulting velocity structure shows strong horizontal variations due to the complicated structure and the variation of crustal thickness. Relatively low-velocity contours are observed in the area defined by Cephallonia—Zakynthos Islands and northwestern Peloponnesos. This is in addition to some well localized peaks of relatively higher values of *P*-wave velocity may be related to the zone of Triassic evaporites in the region and correspond to diapirism that breaks through to the uppermost layer. Finally, a low *P*-velocity 'deeping' zone extending from Zakynthos to the Gulf of Patras is correlated with Bouguer anomaly map and onshore and offshore borehole drillings which indicate that thick sediments overly the evaporites which exist there at depth greater than 2 km.

Key words: Seismic tomography, W. Greece, microearthquake networks.

1. Introduction

The western portion of Greece is the most seismically active area in that country and is characterized by extensive and complex deformation (Fig. 1). The tectonic features that dominate western Greece are: subduction of the African plate beneath the Aegean microplate along the western Hellenic trench (LE PICHON and ANGELIER, 1979, 1981; MCKENZIE, 1972, 1978; MERCIER *et al.*, 1972, 1976, 1987; HATZFELD *et al.*, 1990), the Cephallonia transfer fault at the northwestern end of the Hellenic arc (ANDERSON and JACKSON, 1987; FINNETI, 1976, 1982; UNDERHILL, 1988, 1989), the Adriatic collision which follows to the NW as the Apulia microplate converges with the Aegean (ANDERSON, 1987; ANDERSON and JACKSON, 1987; HATZFELD *et al.*, 1995), and finally the N–S extension which is the main characteristic of the approximately E–W trending grabens (BROOKS *et al.*, 1988;

[1] Seismology Laboratory, University of Patras, Rio 261 10, Greece.
[2] Earthquake Planning and Protection Organization, Xanthou 32, 154 51 Athens, Greece.

Melis *et al.*, 1989, 1995) which forms the inner part of the Hellenic arc (i.e., Trikhonis Lake, Gulf of Patras, Gulf of Corinth, Pyrgos Basin). Diapirism has been observed offshore in the Zakynthos-Cephallonia channels along the lines of reverse faulting, justifying even more the E–W compression which takes place in the area (Brooks and Ferentinos, 1984; Underhill, 1988). Thus, in general, the area of western Greece is characterized by variations in the tectonic regime which should result in complicated structures.

In the present study, the 3-D *P*-wave velocity structure of the area which covers the Ionian Islands of Cephallonia—Zakynthos to the west, the western Peloponnesos to the east and the Gulf of Patras to the north is investigated (Fig. 1). Figure 2 presents the epicentral distribution of seismicity recorded by the University of Patras Seismic Network (PATNET) in 1996. The best constrained events from this local earthquake data set are used in a seismic tomography inversion that results in a 3-D *P*-wave velocity model for the region.

2. The University of Patras Seismic Network (PATNET)

The University of Patras Seismic Network (PATNET) covers all of western Greece (Fig. 3). It commenced operation in the summer of 1991 with six stations around the Gulf of Patras and since the winter of 1995 it has consisted of sixteen outstations and a base station (station coordinates are shown in Table 1). Further expansion of the network is currently under implementation with another eight outstations to be installed by the end of 1997 (Fig. 3). Each outstation is deployed with one vertical component short-period (1 Hz) S-13 seismometer operating in a low-noise environment. Signals are amplified to 60 dB and filtered with a 0.2 Hz high-pass and a 50 Hz low-pass analogue filter. Thereafter, they are radiolinked using FM subcarriers to the central recording site at the Seismology Laboratory of the University of Patras (base station), where a three-component (3 S-13: one vertical and two horizontals N-S/E-W) seismometer station is deployed. There, the signal of each channel is antialias filtered with a 200 Hz Butterworth analogue low-pass filter and it is then converted to digital form sampled at 100 Hz with a 16-bit resolution A/D converter. The standard STA/LTA technique is employed for event triggering. All recorded events are then processed and located according to the following procedure.

For the initial phase picking and data processing, SISMWIN (Tselentis *et al.*, 1994), program developed in-house is used. SISMWIN employs features that are particularly convenient for arrival picking, zooming and noise reduction (i.e., in general filtering of velocity seismogram using user-defined band-pass filters, production of instrument and noise corrected deconvolved displacement seismogram, etc.). Thus, for seismograms with a S/N ratio greater than 5, *P*- and *S*-wave arrival times are read with an accuracy of approximately 0.02 s and 0.07 s, respectively.

For the event location and magnitude calculation, the HYPO71PC program (LEE and LAHR, 1975; LEE and VALDES, 1985) is used. The 1-D velocity model for locating the events is that proposed by TSELENTIS *et al.* (1994) and is used in

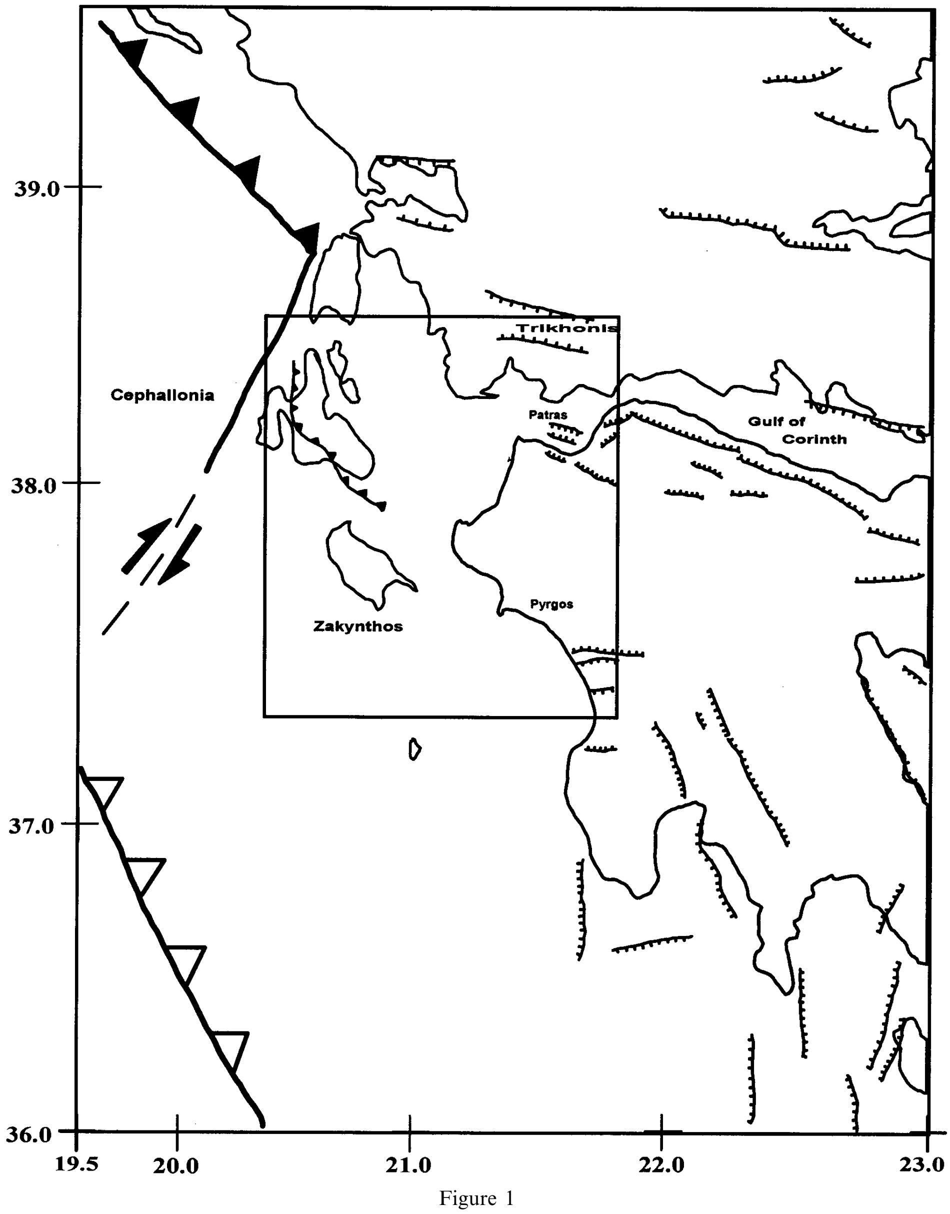

Figure 1
Major tectonic features in Western Greece (after BROOKS *et al.*, 1988; LEPICHON and ANGELIER, 1979, 1981; MERCIER *et al.*, 1972, 1976, 1987; HATZFELD *et al.*, 1990). The box indicates the study area.

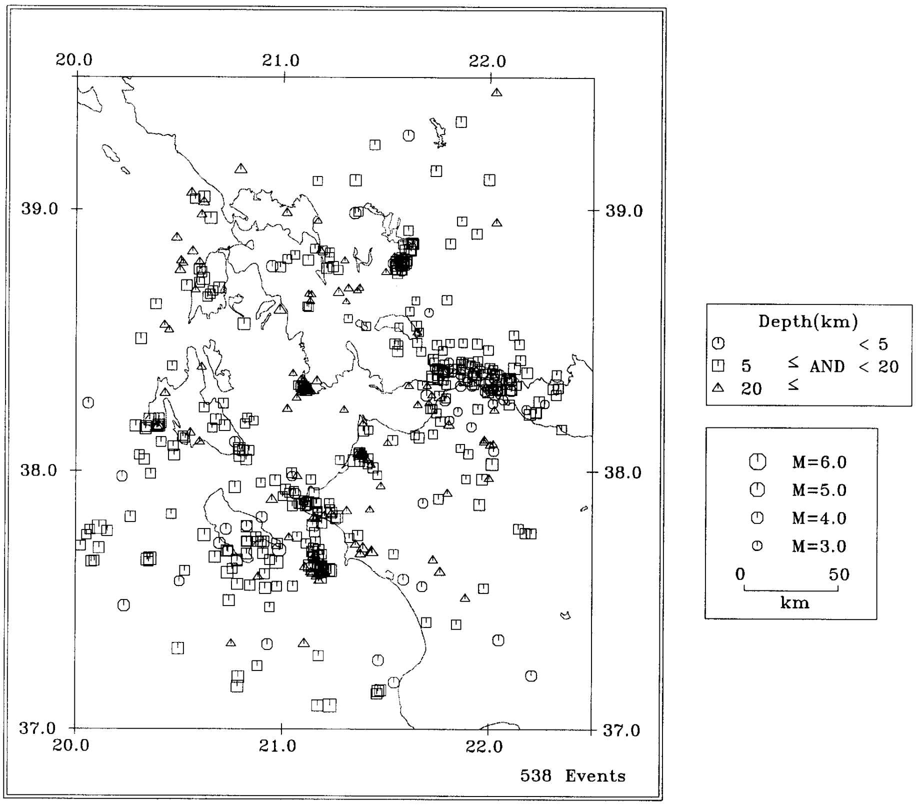

Figure 2
Epicentral distribution of seismicity recorded by PATNET during 1996.

PATNET on a routine basis (Table 2). The magnitude reported for all the events is the local duration magnitude M_L, calculated from total signal duration following LEE *et al.* (1972), applying the equation (after KIRATZI and PAPAZACHOS, 1985; TSELENTIS *et al.*, 1994)

$$M_L = 2.32\log(T) + 0.0013D + C$$

where T is the signal duration in seconds, D is the epicentral distance in km and C a constant, different for each station.

3. Simultaneous Inversion Method

The tomographic inversion method used in the present study is the one developed by THURBER (1981, 1983) for the iterative simultaneous inversion of P-wave arrival-time data for a 3-D crustal velocity structure and hypocentral parameters.The program used was adapted by EBERHART-PHILLIPS (1989, 1990) to include the inversion of *S*-wave data. Thus, *P*- and *S*-wave arrival times can be inverted independently to produce *P*- and *S*-wave velocity models of the upper crust. In this study only *P*-wave arrival-time data were used as PATNET is deployed with only single vertical component seismometers and the *S*-wave arrival times were not accepted as sufficient enough to be used in the present case of inversion (see section on data selection to follow).

Generally the method used comprises the following features:

1) parameter separation (PAVLIS and BOOKER, 1980), which operates on the matrix of hypocentral and velocity partial derivatives which enable the separation of the velocity and hypocentral calculations into equivalent subsets of equations which are computationally manageable.

2) the approximate ray-tracing method (ART), which requires little computational time to permit an iterative solution to the problem (THURBER, 1983). It

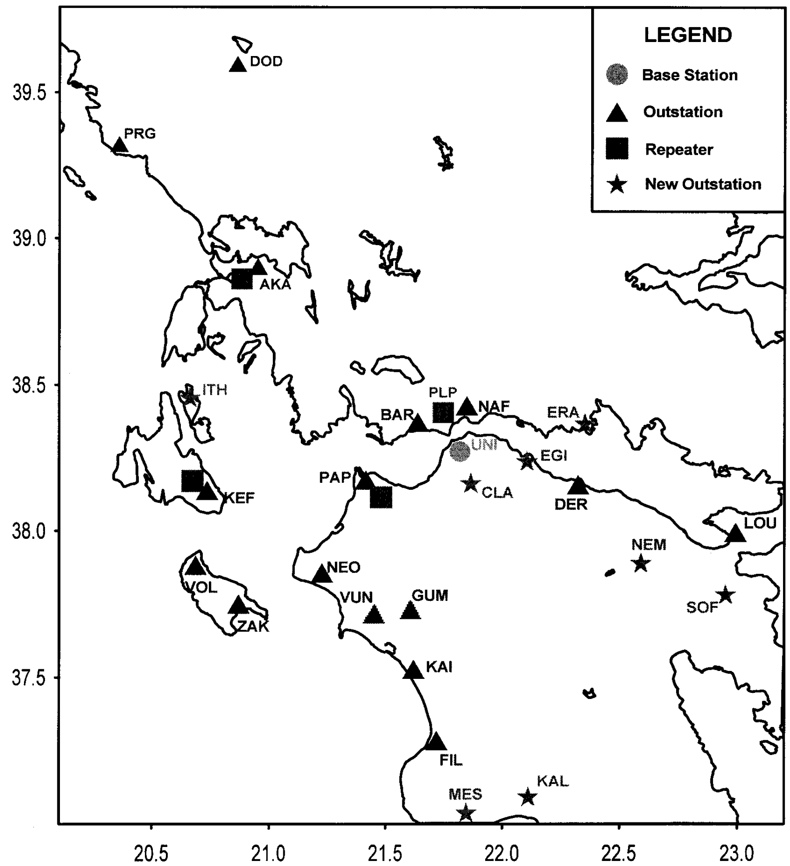

Figure 3
Present station distribution of the University of Patras Seismic Network (PATNET).

Table 1

PATNET Station details

No.	St. Id.	Lat. (°N-′)	Lon. (°E-′)	Altit. (m)
1	UNI	38 17.35	21 47.32	70
2	NAF	38 25.00	21 51.57	280
3	BAR	38 21.10	21 36.45	340
4	PAP	38 11.38	21 24.81	196
5	AKA	38 48.50	20 59.02	1440
6	ZAK	37 43.58	20 49.51	200
7	KEF	38 6.60	20 47.30	507
8	FIL	37 8.81	21 37.20	340
9	VOL	37 53.22	20 40.72	450
10	VUN	37 44.47	21 23.59	240
11	GUM	37 45.35	21 37.19	367
12	NEO	37 54.43	21 9.55	100
13	DER	38 6.09	22 24.55	410
14	LOU	37 59.42	22 58.50	300
15	KAI	37 31.55	21 35.65	10
16	DOD	39 29.01	20 42.03	760
17	PRG	39 19.35	20 21.41	512

constructs a set of smooth curves connecting the earthquake ‘source’ and the ‘receiver’ station, and numerically calculates the travel time along each curve. Arcs of varying radii are examined and the dip of the plane containing the arcs is varied systematically. An approximation to the true ray path is selected as being that with the shortest travel time. For paths which are fairly short (<50 km) the travel time estimated by this method agrees well with the ‘true’ ray path travel time calculated using a 3-D ray tracer. Hypothetical models tested to date give a standard deviation of 0.02 s (THURBER, 1983). This method is however limited in that the path curvature is constant along a given curve and that each curve lies within a single plane. Pseudobending is used to perturb the ‘ART’ ray path to satisfy the criteria that the direction of the true ray path curvature is antiparallel to the component of the local velocity gradient normal to the path at each point. This enables a given ray to have varying curvature and to deviate from a single plane (THURBER, 1983).

Table 2

V_p crustal velocity model used for 1-D earthquake location

Velocity (km/sec)	Depth (km)
5.7	0.0
6.0	5.0
6.4	18.0
7.9	39.0

Table 3

Hypocentral details of the 168 selected events

Date	Origin	Lat. N	Long. E	Depth	Mag.
960106	641 18.15	38-14.43	21-43.45	18.40	2.94
960110	17 9 48.30	38- 8.56	21-43.69	17.56	2.90
960123	1010 39.41	38-23.36	21-51.67	10.55	2.97
960128	21 6 32.68	38-22.83	21-46.34	7.10	3.19
960308	2245 37.64	38-29.04	21-44.67	11.58	3.24
960310	1745 59.04	38- 4.02	21-53.88	18.35	3.02
960317	638 18.34	38-18.95	21- 5.62	23.08	4.15
960322	4 0 41.35	38-18.32	21-59.58	7.20	3.83
960326	134 35.86	38-22.33	21-51.67	4.86	3.24
960406	856 36.56	38-40.97	21-16.08	20.46	3.96
960423	1721 46.38	38-46.05	20-30.17	29.90	3.87
960504	1141 59.99	38- 2.65	20-49.37	14.20	3.72
960505	3 4 29.62	38-30.37	20-18.88	17.50	3.84
960509	226 43.68	38-14.41	21-42.80	17.99	3.10
960518	1232 28.31	38-10.21	20-20.42	13.21	3.82
960526	2144 19.17	38-10.00	20-23.51	22.72	4.71
960529	1327 11.76	38-11.86	20-40.65	12.24	3.68
960530	1026 34.66	38-52.24	21-37.45	16.63	4.02
960531	252 8.16	37-34.94	21-35.18	3.35	3.62
960601	924 29.23	38-10.44	20-24.11	17.17	4.19
960601	1227 16.55	37-36.61	21-45.78	24.67	3.92
960606	1625 36.20	37-37.16	21-13.44	15.81	4.68
960607	814 3.08	37-35.93	21-11.36	28.92	3.63
960611	551 56.56	38-17.51	21-41.74	4.59	3.82
960611	12 6 44.13	38-21.20	21-44.83	5.92	3.13
960613	541 23.28	37-36.93	21-13.98	17.55	4.45
960614	2336 17.41	37-37.69	21-10.66	27.99	4.02
960615	19 6 3.77	37-45.15	21-21.88	15.49	3.63
960618	142 31.83	38-27.56	21-33.27	17.87	3.58
960620	220 45.09	37-43.68	20-54.49	7.30	3.75
960621	8 2 56.70	37-52.54	21- 4.91	16.80	3.61
960621	857 26.36	37-35.23	21-11.34	18.50	3.70
960621	17 1 53.20	37-39.48	20-46.90	13.43	3.84
960621	1736 54.11	37-40.85	20-49.61	10.80	3.58
960623	2230 35.56	38-39.18	21-38.49	12.94	2.55
960624	2339 37.33	38-15.20	21-39.15	26.83	3.08
960627	1353 38.73	38-23.76	21-44.10	2.47	3.13
960629	1025 31.11	37-36.37	21-10.95	26.43	3.77
960629	1416 29.98	37-35.68	21-10.03	27.70	3.85
960630	451 53.52	38- 5.16	20-47.40	17.07	4.15
960704	2157 19.12	38-10.30	20-24.03	25.48	4.58
960704	2225 15.70	38-11.83	20-21.48	13.01	4.08
960708	2334 37.50	37-10.02	20-47.11	13.57	4.15
960709	1422 10.50	37-43.28	20-41.80	0.17	3.91
960710	2253 7.69	37-39.16	20-46.85	17.13	3.69
960717	19 3 0.97	37-58.77	21- 4.18	26.23	3.46
960718	1432 29.59	37-57.85	20-57.87	17.16	3.70
960719	1853 40.38	37-52.95	21- 7.62	13.10	3.45
960723	717 53.25	38- 3.68	20-28.56	16.95	3.77

Table 3 *continued*

Date	Origin	Lat. N	Long. E	Depth	Mag.
960727	2350 9.39	37-36.47	20-44.06	16.32	4.14
960801	031 23.88	37-47.52	21- 8.74	15.20	3.98
960801	922 9.47	37-40.32	21-10.32	17.99	4.04
960804	1741 14.49	37-36.79	21-11.06	25.73	4.52
960805	513 33.90	37-49.36	20-54.00	4.38	3.79
960806	2217 26.64	37-58.15	21-57.93	13.57	3.69
960806	2345 52.72	38-22.89	21-46.67	6.26	4.01
960810	1522 21.24	37-47.17	20-49.61	7.15	3.93
960810	23 5 24.72	37-39.49	20-20.88	9.00	4.21
960811	1143 44.80	37-41.22	21-25.88	23.71	4.74
960811	1241 38.68	37-41.15	21-26.18	26.34	4.03
960811	2148 56.11	38- 4.23	21-23.26	22.13	3.23
960811	2312 46.78	38- 4.00	21-22.85	21.19	3.08
960812	027 35.53	38- 3.79	21-22.72	22.22	3.25
960812	340 54.05	38- 3.72	21-23.07	19.41	2.89
960813	2151 19.34	38- 9.75	20-20.28	13.22	3.93
960814	9 9 54.00	38- 3.82	21-22.97	23.50	3.43
960815	8 2 50.12	38- 4.37	21-22.96	22.22	3.45
960815	82 9.84	38- 3.75	21-22.69	23.49	3.56
960815	1416 23.67	38- 4.11	21-22.99	24.85	3.47
960815	1437 39.30	38- 3.87	21-22.39	21.53	3.48
960815	1440 53.13	38- 1.54	21-24.67	19.95	2.81
960815	1446 58.13	38- 3.91	21-22.11	19.45	3.66
960815	1459 13.02	38- 0.82	21-26.25	18.73	3.45
960815	23 4 53.17	38- 2.77	21-23.50	21.33	3.11
960815	2316 38.42	38-22.67	22- 0.63	13.84	3.04
960816	1910 36.63	38- 3.91	21-23.20	21.19	3.33
960816	2148 46.38	38- 3.86	21-21.62	24.82	3.05
960816	2228 52.25	38- 4.22	21-22.32	17.40	3.55
960818	1343 41.60	37-38.13	21- 7.82	17.74	3.98
960819	3 8 44.57	37-36.09	21-10.37	23.02	4.15
960819	2155 55.89	37-36.56	21- 8.28	28.08	3.48
960821	231 9.34	38-10.97	21-23.27	20.28	2.62
960822	2 0 59.60	38-23.21	21-46.67	13.93	4.22
960823	1119 6.92	38-23.64	21-44.15	1.06	3.15
960823	2147 56.61	38-23.33	21-44.67	1.43	2.94
960824	636 15.41	38-17.45	21-45.40	7.20	3.29
960824	1732 45.85	37-52.49	21- 9.65	7.34	3.62
960824	2326 35.07	37-43.21	20-58.49	10.94	3.60
960825	143 28.99	38-23.13	21-46.58	11.20	3.09
960825	2253 23.13	38- 5.96	22- 0.24	20.18	3.31
960826	1612 5.04	37-32.89	20-55.02	15.46	4.00
960826	20 0 57.24	38- 9.34	21-23.42	16.19	3.59
960827	2134 5.31	38-46.94	21-14.44	13.54	3.54
960828	1222 9.45	37-42.09	21-23.40	25.31	4.44
960828	1226 56.55	37-40.79	21-22.67	24.24	3.66
960831	348 5.89	38-23.60	21-45.01	12.15	3.38
960831	925 31.87	38-21.61	21-53.60	7.10	3.29
960831	1443 34.20	37-37.37	21- 8.75	15.50	4.28
960831	1813 17.10	38-14.00	22- 1.45	53.77	3.24

Table 3 continued

Date	Origin	Lat. N	Long. E	Depth	Mag.
960831	19 1 30.02	37-40.05	21- 9.13	19.67	3.63
960905	147 12.62	38-29.30	21-32.46	12.65	3.51
960906	1037 54.96	38- 7.16	21-31.89	16.23	3.36
960909	1849 38.91	37-45.20	20-37.35	13.64	4.42
960911	1859 18.53	38-22.68	22-10.90	13.67	3.70
960915	1358 50.85	37-36.87	21-11.42	16.70	4.08
960915	1859 1.36	37-37.82	21-11.10	16.80	3.73
960915	2150 54.12	37-36.92	21-11.94	16.08	3.68
960916	2132 33.33	38-29.55	21-38.92	10.89	3.03
960918	625 14.09	38- 8.18	21-56.75	12.41	3.04
960918	1337 1.68	37-52.33	21-57.19	7.58	3.90
960920	2018 7.55	38-16.90	21-47.42	5.21	2.94
960921	1629 30.61	38-37.83	21- 6.87	19.00	2.85
960922	1452 6.90	38-37.68	21- 7.39	17.34	3.12
960930	038 17.74	38-10.50	20-43.15	19.25	3.70
961001	1016 55.34	38-21.20	21-43.35	8.66	3.70
961001	2039 27.93	37-55.78	21- 0.88	17.68	3.35
961003	10 7 27.29	38- 6.70	20-45.83	4.51	3.49
961008	1746 54.72	38-25.56	22- 8.99	18.71	3.34
961009	7 8 7.84	38- 7.75	21-39.59	19.38	3.46
961009	1127 42.78	37-54.95	21- 1.87	15.82	2.94
961010	2031 35.75	37-51.15	21-13.82	10.23	3.15
961011	210 24.45	38- 4.96	20-47.40	10.68	3.24
961011	11 0 46.08	38- 4.72	20-48.40	10.92	3.66
961012	311 26.25	38-48.29	21-17.82	33.14	2.80
961012	22 2 36.69	37-54.87	21-47.88	28.74	3.29
961013	451 49.63	38- 8.37	21-38.34	16.41	2.79
961013	9 4 8.12	38-23.10	21-48.02	14.59	3.28
961016	1048 33.85	37-39.29	22-42.37	5.89	3.93
961016	1125 1.40	37-51.92	21- 6.59	17.35	3.25
961018	720 58.85	38-27.76	21-46.39	12.49	2.79
961018	1819 10.86	37-45.66	22-12.34	16.40	3.34
961022	1016 4.85	37-42.99	21-21.24	27.39	3.52
961023	1055 17.16	38-11.79	21-48.37	4.32	2.73
961023	12 7 39.97	37-12.21	20-47.34	18.11	4.17
961023	1432 40.73	37-56.50	21-28.51	24.02	3.08
961023	1459 28.70	37-41.52	20-43.93	17.85	3.95
961028	2251 59.73	37-48.94	21- 9.65	22.12	3.59
961028	2317 27.29	37-49.07	21- 9.06	25.01	4.02
961101	1 5 46.32	37-54.99	21- 9.18	12.33	3.35
961102	1841 0.33	38-25.02	21-53.84	7.52	3.12
961105	133 31.12	38-47.67	20-31.00	24.55	3.32
961107	4 4 59.29	37-44.60	21- 1.91	28.01	3.17
961107	2254 11.67	38-23.35	22- 1.08	10.63	3.14
961108	911 24.77	38-27.87	21-59.64	17.95	3.25
961110	619 49.19	38- 2.46	21-20.65	13.35	4.11
961110	1118 27.31	37-52.39	21- 5.29	16.08	3.16
961113	931 37.33	37-39.66	20-21.66	8.83	4.54
961113	11 6 59.95	37-28.79	20-14.20	4.51	4.05
961115	639 56.34	38-18.54	22- 6.36	4.64	3.38
961115	1321 46.76	37-47.94	21-11.41	16.22	3.47
961116	1738 18.23	38-21.10	22- 2.61	8.79	3.75

Table 3 continued

Date	Origin	Lat. N	Long. E	Depth	Mag.
961120	1927 35.17	38- 4.67	22- 1.28	3.52	3.15
961125	1747 51.64	37-25.07	21-41.91	14.35	3.26
961127	241 9.70	38- 6.47	21-30.45	24.22	2.89
961201	4 9 44.48	38-16.48	22- 4.03	1.55	2.94
961201	613 45.01	38-19.61	21-36.60	22.83	2.98
961205	740 26.30	38-21.84	21-43.41	5.68	4.02
961208	2325 9.46	37-51.06	21-25.39	60.69	2.86
961214	759 8.79	38-10.27	21-54.79	2.08	3.03
961216	8 7 43.48	38-21.04	21- 5.25	30.67	2.96
961216	16 9 53.80	38-20.72	21- 9.88	33.40	3.67
961216	1620 50.65	38-20.82	21- 6.13	26.99	2.86
961217	1324 47.02	38-56.96	22- 1.89	86.39	3.53
961226	14 7 1.79	38-29.27	21-56.39	17.45	3.47
961226	2123 52.68	38-54.48	21-56.22	15.36	3.43
961227	2133 36.02	37-53.32	20-56.89	27.00	4.22
961228	1149 27.01	38-50.35	20-33.76	20.81	3.70
961228	2338 24.34	38-52.21	21-48.50	5.23	3.37

3) velocity model parameterization. This is achieved by assigning velocity values at fixed points on a 3-D grid. A continuous velocity field is assumed by linearly interpolating between the specified grid points for velocity values along the ray paths and for velocity partial derivatives. This produces a solution with gradational changes in velocity rather than imposing sharp discontinuities by using block models. Thus, contouring of the final solution enables identification of 3-D velocity structures.

The program iterates to find a damped least-squares solution using singular value decomposition. A damping parameter, defined by the user, is added to the diagonal elements of the separated medium matrix in order to prevent large model changes which would occur for near zero singular values. If the damping parameter is too small the velocity values oscillate from one grid point to another, causing large changes in velocity to occur without a corresponding reduction in the data variance. The idea is to reduce the data variance without increasing the solution variance significantly (i.e., to reduce the travel-time residual variance without introducing large velocity variations). Traditionally, the damping parameter is chosen to equal the ratio of the data variance to the model variance (EBERHART-PHILLIPS, 1989). In this study, empirical testing of damping parameters was also performed, by running inversions with different damping values. Hence, the value of 25 for P-wave data was selected. Convergence to a solution is checked by calculating the ratio of the previous data variance to the new data variance after each iteration.

A 95% F-test is applied in the usual manner to decide if the new result is significant. The F-test is a test of the significance of the error improvement, that is whether the improvement is too large to be accounted for by random fluctuations in the data and is therefore significant (MENKE, 1984). This study required four iterations to converge to a solution.

4. P-Wave Tomography Study in Western Greece

(a) Event Selection

The PATNET data set of events which occurred in 1996 was first selected from the entire set of 2,500 events that occurred in 1991–1996. 538 events were included in the resultant 1996 data set and their epicentral distribution is shown in Figure 2. For the present study a smaller subset of 168 events was selected on the basis of the following critera:

1) the quality of the P-arrival time picking. Only the events with at least ten observations of zero weight were selected.

2) the total RMS travel-time residual. For each selected event this was less than 0.20 s.

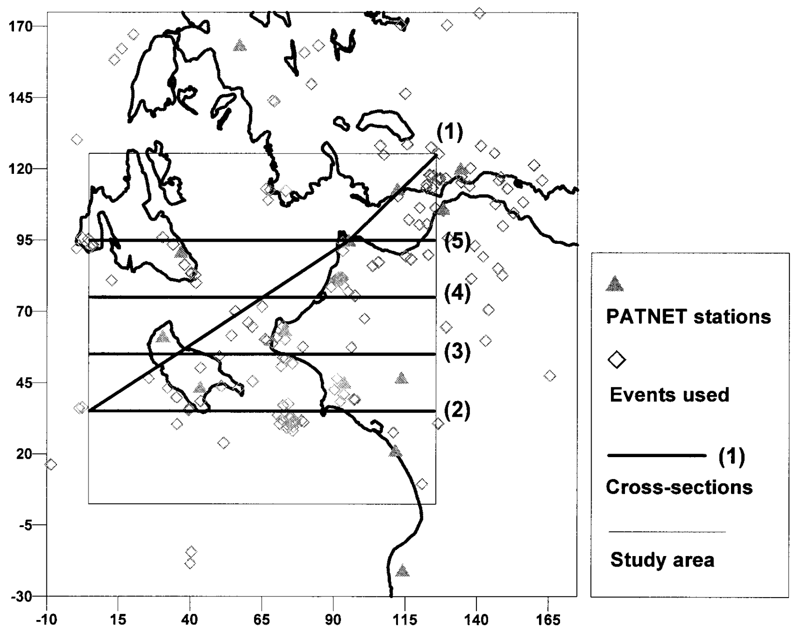

Figure 4
Epicentral distribution of the 168 selected events for inversion. The area selected for inversion is noted with the box. Cross-sections contoured and presented in Figures 8–9 are shown with solid lines and numbers.

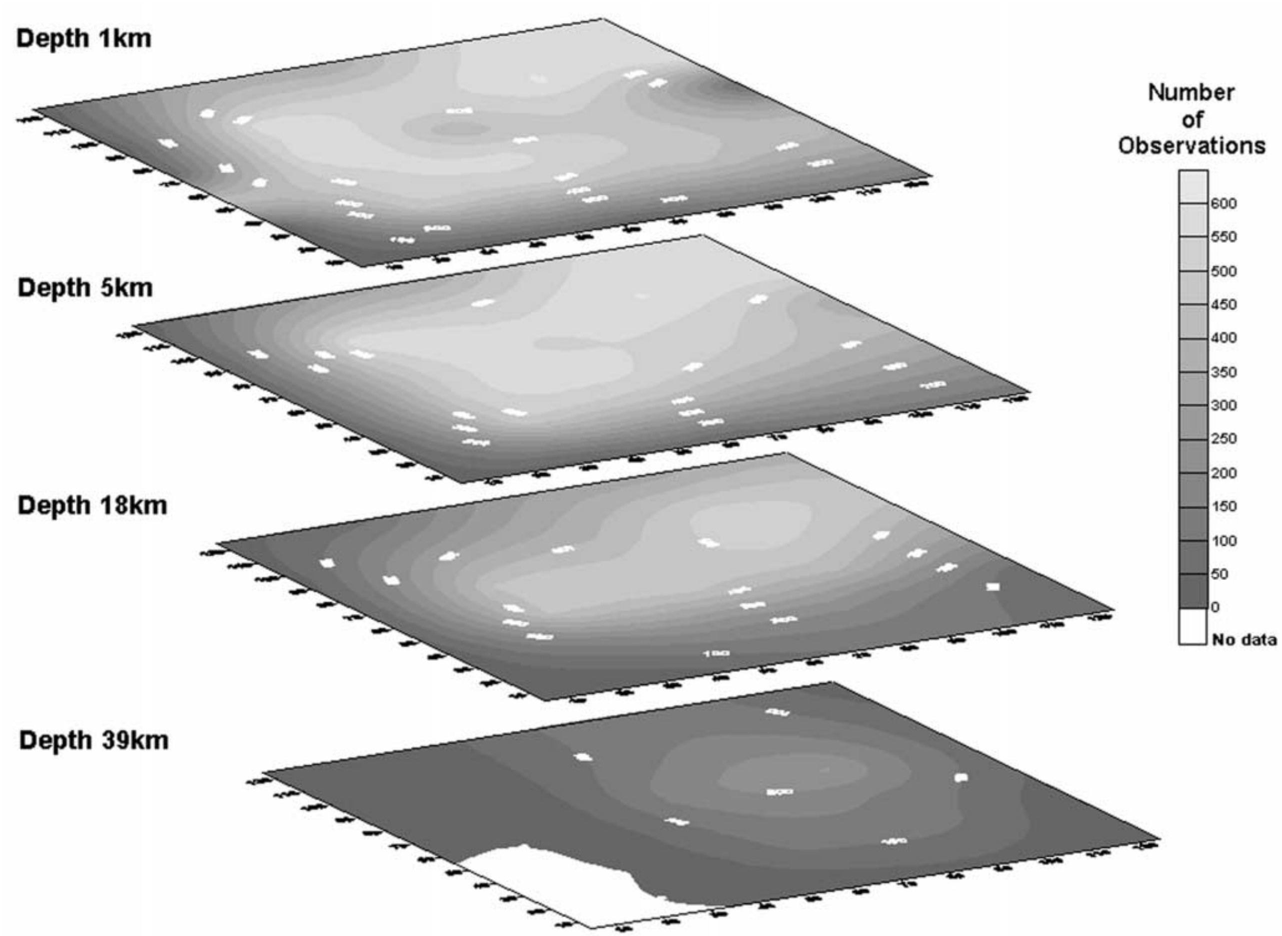

Figure 5

Contours of the number of observations for each grid and for each defined layer.

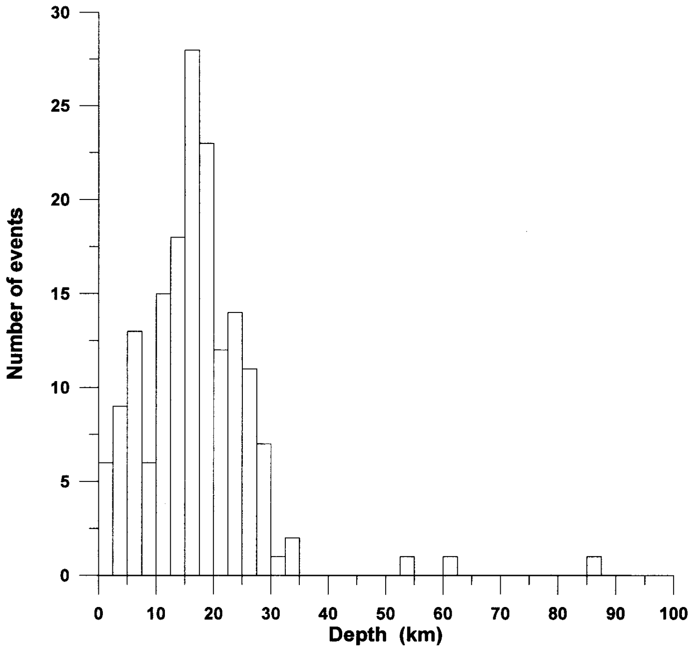

Figure 6
Histogram showing depth distribution of the 168 events selected for inversion.

3) the uncertainty in the epicenter and focal depth. The locations for the events selected were allowed an error less than 4 km on both epicenters and focal depth determinations.

4) the spatial distribution of the epicenters of selected events. Special care was taken to aim for a distribution of the most evenly possible epicenters of events throughout the study area.

168 events were found that met the above criteria. Their hypocentral details and local magnitudes are given in Table 3 and their epicentral distribution is shown in Figure 4.

(b) Velocity Model Used

The initial velocity model used in the present inversion study was adopted from the 1-D model which is used routinely in PATNET and is presented in Table 2. A grid was defined with origin the point with coordinates: latitude 37°20′ N, longitude 20°20′ E. This was the (0,0) point of the defined grid with dimensions 125 × 125 km (Fig. 4). The grid nodes were not evenly spaced at x and y axes, but were defined for x at: 5, 35, 65, 95 and 125 km and for y at: 5, 35, 55, 75, 95, 125 km

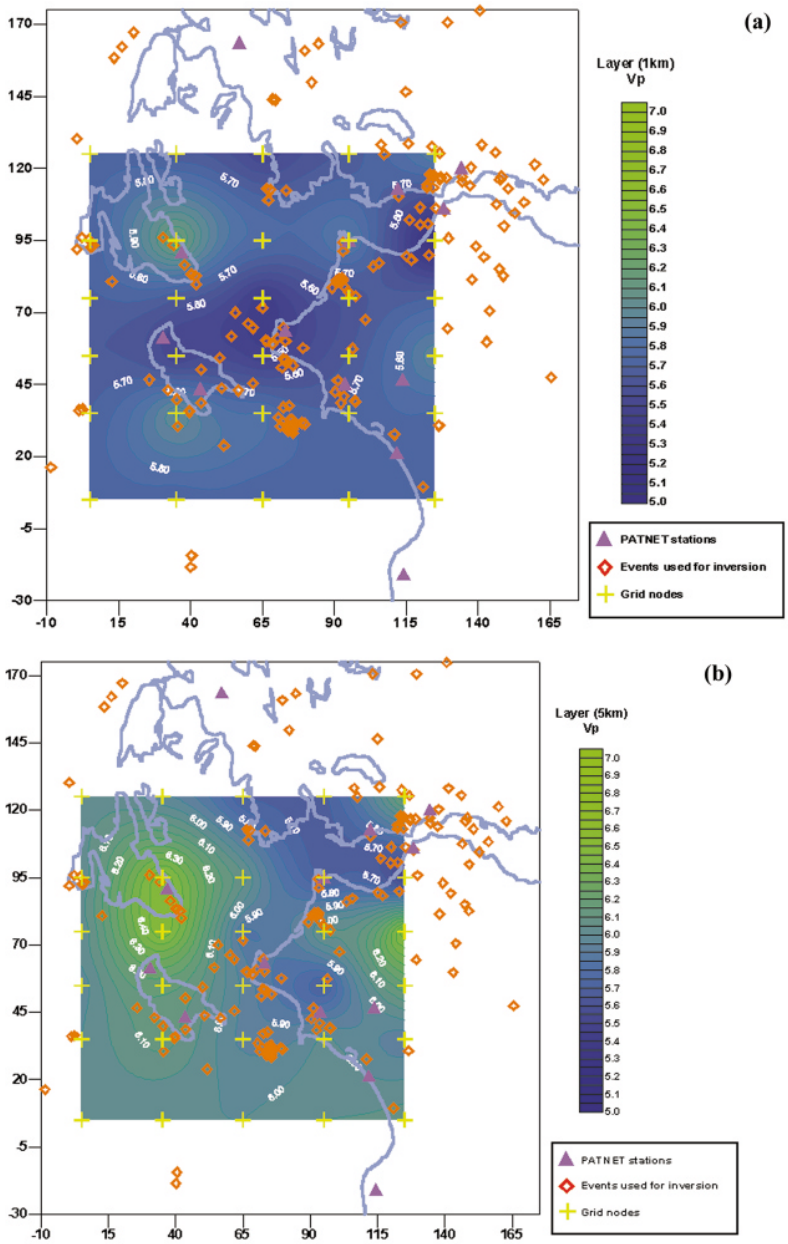

Figure 7

P-wave velocity contour diagrams for: (a) layer at 1 km, (b) layer at 5 km, (c) layer at 18 km depth, respectively.

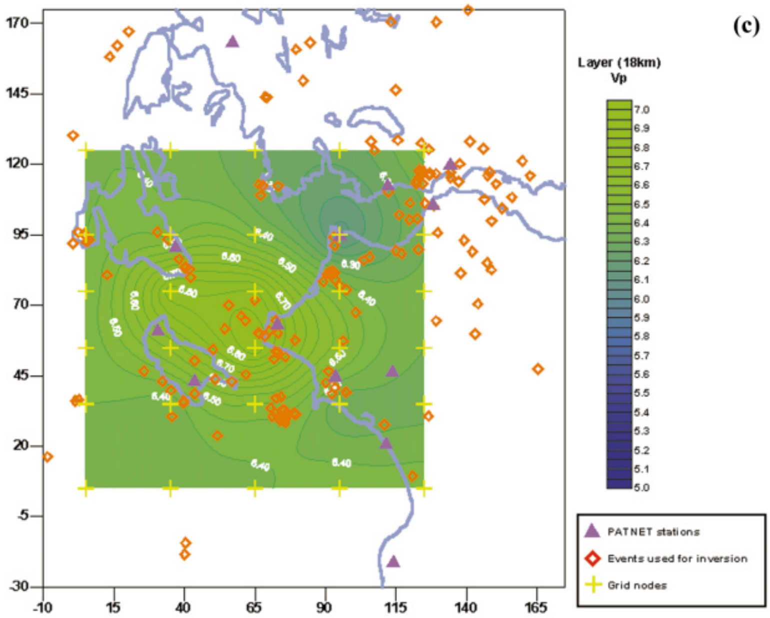

Figure 7 (continued).

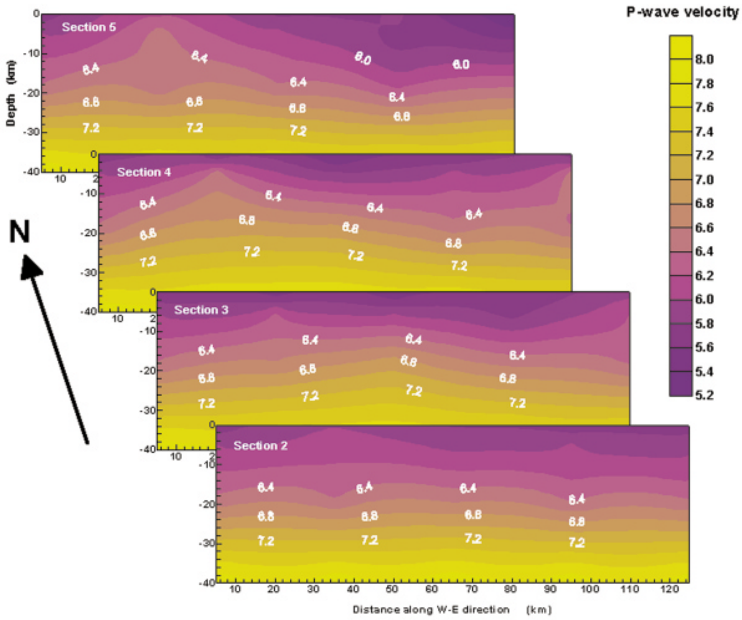

Figure 8

P-wave velocity contour diagrams for cross-sections 2–5 shown in Figure 4.

respectively. Four layers of these grid points at 1, 5, 18 and 39 km depth were defined according to the 1-D model in Table 2 and were assigned P-wave velocities, respectively. Thus a volume of $125 \times 125 \times 38$ km^3 was defined in the area of western Greece.

(c) Resolution

A resolution matrix is produced at the end of the inversion procedure which indicates how well the velocity is constrained at each grid node, as it is correlated to the number of rays passing at each grid node (THURBER, 1983). Figure 5 presents for each grid layer, contours of the number of rays passing at each grid node. It can be seen that only for layer 4, at 39 km depth the coverage is not sufficient. This is due to the focal depth coverage of events used in the present inversion study, which as it is shown in the histogram of Figure 6 corresponds to depths shallower than 20 km. Thus, the resolution should also increase at depths shallower than 20 km. In general for the present study the resolution values for the P-wave velocity model were in the range of 0.0 to 0.62 with an average of 0.24. It is observed here as is also shown in Figure 5 that the resolution is poor at depths greater than 20 km and at the western and southern parts of the layer at 18 km.

(d) Resulting P-wave Velocity Model

The resulting values for each layer were contoured using a grid spacing of 2.5 km in both the x and y directions (Figs. 7a–c). Cross-sections were also selected as illustrated in Figure 4 and they were also contoured using a grid spacing of 2.5 km at the x and z directions (Fig. 8). Finally, a cross-section, noted as 1 in Figure 4 was also selected and the resulting contours are shown in Figure 9.

Viewing Figures 7–9, a well-defined localized anomaly of low P-wave velocity can be observed at the Cephallonia—Zakynthos—NW Peloponnesos area. This coincides with intrusions of local diapirs which were observed by BROOKS and FERENTINOS (1984) and also presented by UNDERHILL (1988). The evaporitic outcrop in the area is shown in Figure 10 (from UNDERHILL, 1988 and after BROOKS and FERENTINOS, 1984). The line of seismic section and its interpretation are shown in Figure 10 and it runs obliquely through sections 1, 4 and 5 (Figs. 8, 9) where the localized relatively low P-velocity contours can be seen.

It is also interesting to emphasize the appearance of a low P-wave velocity "deeping" zone which is developed towards the Gulf of Patras (Figs. 7a, b, 8 and 9). There, offshore drilling by the Public Petroleum Corporation of Greece proved that thick sediments of 1800 m overlie the Triassic evaporites (FERENTINOS *et al.*, 1985; BROOKS *et al.*, 1988). The later have also been found

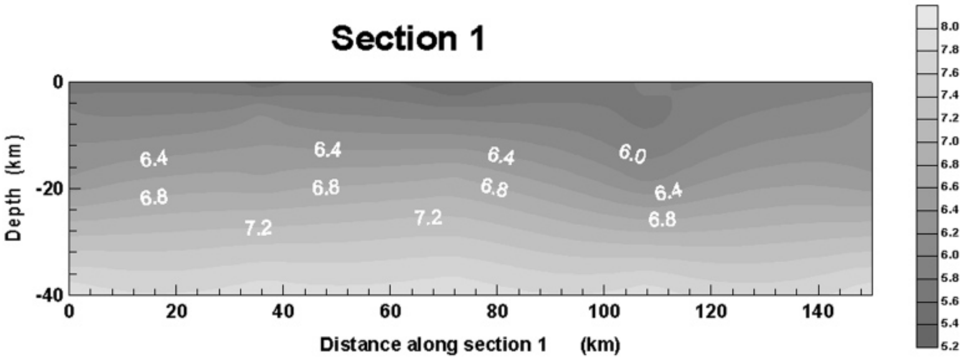

Figure 9
P-wave velocity contour diagram for cross-section 1 shown in Figure 4. Note the low *P*-wave velocity zone 'deeping' towards the Gulf of Patras.

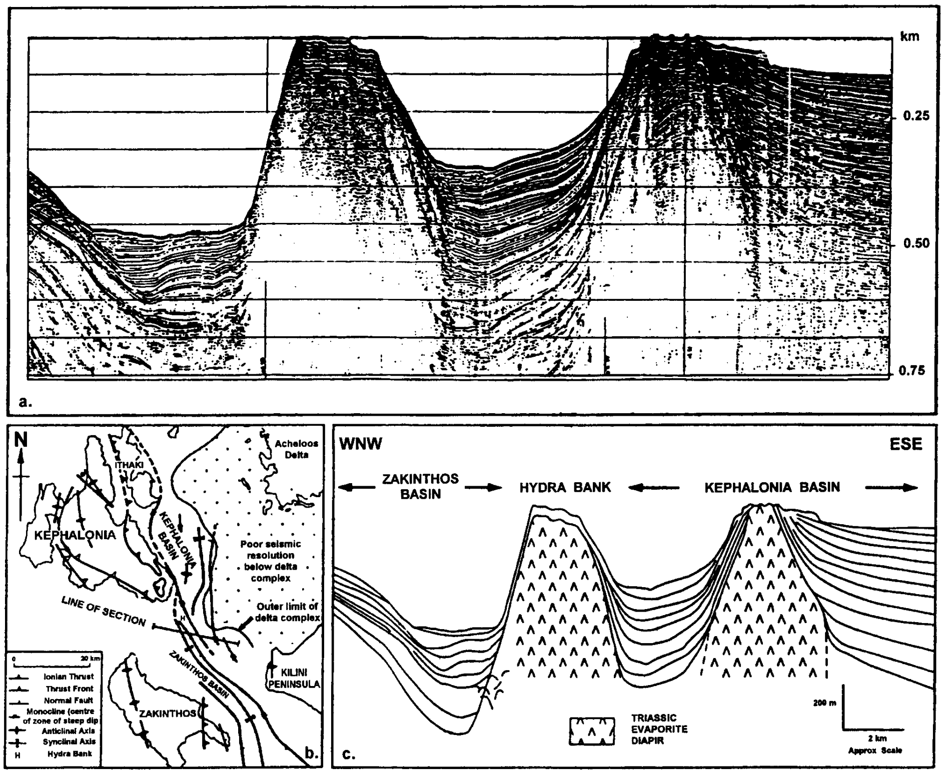

Figure 10
(a) Single channel air-gun record across Zakynthos and Cephallonia Basins. (b) and (c) location and interpretation respectively emphasizing the Triassic evaporite diapirs (from UNDERHILL, 1988 and after BROOKS and FERENTINOS, 1984).

in onshore drilling at depths of about 2500 m (BP Co. Ltd., 1971) North of the Gulf of Patras. Thus the combination of evaporites and thick sediments towards the Gulf of Patras define a thicker low-velocity layer.

5. Conclusions

The present investigation of *P*-wave velocity in the area of western Greece demonstrates the importance of 3-D-inversion studies in areas of high seismic activity. An estimate of the locations of relatively low velocity areas in the region is also given. The existence of these relatively low velocity rocks provides important input that is necessary to achieve accurate earthquake locations. A future extended study, using a larger number of events, will be extremely useful for improving earthquake locations in the region. Existing off-shore seismic profiles only provide information for shallower depths, nonetheless these are useful for modeling shallow structures (i.e., evaporitic intrusions which are also outcrop in the area). Lastly, borehole information (BP Co. Ltd., 1971) and gravity data (BROOKS *et al.*, 1988) can also be utilized in order to correlate a more detailed model which can be produced for the studied area.

Acknowledgments

We are grateful to Drs. P. Maguire and P. W. Burton for their continuous encouragement during this study. Professor B. J. Mitchell and an anonymous reviewer provided useful suggestions for improving the presentation of this work.

REFERENCES

ANDERSON, H. (1987), *Is the Adriatic an African Promontory?* Geology *15*, 212–215.

ANDERSON, H., and JACKSON, J. (1987), *The Deep Seismicity of the Tyrrhenian Sea*, Geophys. J. R. astr. Soc. *91*, 613–637.

BRITISH PETROLEUM COMPANY LTD. (BP CO. LTD.) (1971), *The Geological Results of Petroleum Exploration in Western Greece*, Spec. Rep. Inst. Geol. Geophys. Res. Athens, *10*, 73 pp.

BROOKS, M., and FERENTINOS, G. (1984), *Tectonics and Sedimentation in the Gulf of Corinth and the Zakynthos and Kefallinia Channels, Western Greece*, Tectonophysics *101*, 25–54.

BROOKS, M., CLEWS, J., MELIS, N. S., and UNDERHILL, J. (1988), *Structural Development of Neogene Basins in Western Greece*, Basin Research *1*, 129–138.

CHRONIS, G., PIPER, D. J. W., and ANAGNOSTOU, C. (1991), *Late Quaternary Evolution of the Gulf of Patras, Greece: Tectonism, Deltaic Sedimentation and Sea-level Change*, Mar. Geol. *97*, 181–209.

EBERHART-PHILLIPS, D. (1989), *Investigations of Crustal Structure and Active Tectonic Processes in the Coast Ranges, Central California*, Ph.D. Thesis, Stanford University, California.

EBERHART-PHILLIPS, D. (1990), *Three-dimensional P- and S-velocity Structure in the Coalinga Region California*, J. Geophys. Res. *95*, 15343–15363.

FERENTINOS, G., BROOKS, M., and DOUTSOS, T. (1985), *Quaternary Tectonics in the Gulf of Patras, Western Greece*, J. Struct. Geol. *7*, 713–717.

FINNETI, I. (1976), *Mediterranean Ridge, A Young Submerged Chain Associated with the Hellenic Arc*, Boll. Geofis. Teor. Applic. *15*, 263–341.

FINNETI, I. (1982), *Structure, Stratigraphy and Evolution of the Central Mediterranean Sea*, Boll. Geofis. Teor. Applic. *24*, 247–312.

HATZFELD, D., KASSARAS, I., PANAGIOTOPOULOS, D., AMORESE, D., MAKROPOULOS, K., KARAKAISIS, G., and COUTANT, O. (1995), *Microseismicity and Strain Pattern in Northwestern Greece*, Tectonics *14*, 773–785.

HATZFELD, D., PEDOTTI, G., HATZIDIMITRIOU, P., and MAKROPOULOS, K. (1990), *The Strain Pattern in the Western Hellenic Arc Deduced from a Microearthquake Survey*, Geophys. J. Int. *101*, 181–202.

KIRATZI, A. A., and PAPAZACHOS, B. C. (1985), *Local Richter Magnitude and Total Signal Duration in Greece*, Annal. Geophys. *3*, 531–538.

LEE, W. H. K., BENNET, R. E., and MEAGHER, K. L. (1972), *A Method of Estimating Magnitude of Local Earthquakes from Signal Duration*, U. S. Geological Survey, Open File Report 1–28.

LEE, W. H. K., and LAHR, J. C. (1975), *HYPO71 (Revised): A Computer Program for Determining Hypocentre, Magnitude, and First Motion Pattern of Local Earthquakes*, U.S. Geological Survey, Open File Report 75–311.

LEE, W. H. K., and VALDES, C. M. (1985), *HYPO71PC: A Personal Computer Version of the HYPO71 Earthquake Location Program*, U.S. Geological Survey, Open File Report 85–749.

LE PICHON, X., and ANGELIER, J. (1979), *The Hellenic Arc and Trench System: A Key to the Neotectonic Evolution of the Eastern Mediterranean Area*, Tectonophysics *60*, 1–42.

LE PICHON, X., and ANGELIER, J. (1981), *The Aegean Sea*, R. Soc. Lond. Phil. Trans. *A300*, 357–372.

MCKENZIE, D. P. (1972), *Active Tectonics of the Mediterranean Region*, Geophys. J. R. Astr. Soc. *30*, 109–185.

MCKENZIE, D. P. (1978), *Active Tectonics of the Alpine-Himalayan Belt: The Aegean Sea and Surrounding Regions*, Geophys. J. R. Astr. Soc. *55*, 217–254.

MELIS, N. S., BROOKS, M., and PEARCE, R. G. (1989), *A Microearthquake Network in the Gulf of Patras Region, Western Greece, and its Seismotectonic Interpretation*, Geophys. J. R. Astr. Soc. *98*, 515–524.

MELIS, N. S., BURTON, P. W., and BROOKS, M. (1995), *Coseismic Crustal Deformation from Microseismicity in the Patras Area*, Geophys. J. Int. *122*, 815–836.

MENKE, W., *Geophysical Data Analysis: Discrete Inverse Theory* (Academic Press Inc., New York 1984).

MERCIER, J.-L., SOREL, D., and SIMEAKIS, K. (1987), *Changes in the State of Stress in the Overriding Plate of a Subduction Zone: The Aegean Arc from the Pliocene to the Present*, Annal. Tecton. *1*, 20–39.

MERCIER, J.-L., CAREY, E., PHILIP, H., and SOREL, D. (1976), *La Neotectonique Plio-Quaternaire de l'Arc Egeen Externe et de la Mer Egee et ses Relations avec Seismicite*, Bull. Soc. Geol. Fr. *18*, 159–176.

MERCIER, J.-L., BOUSQUET, B., DELIBASIS, N., DRAKOPOULOS, I., KERAUDREN, B., LEMEILLE, F., and SOREL, D. (1972), *Deformations en Compression dans le Quaternaire des Rivages Ioniennes (Cephalonie, Greece)*, Donnees Neotectoniques et Seismiques, Academie de Sciences Comptes Rendus *275*, 2307–2310.

PAVLIS, G. L., and BROOKER, J. R. (1980), *The Mixed Discrete-Continuous Inverse Problem: Application to the Simultaneous Determination of Earthquake Hypocentres and Velocity Structure*, J. Geophys. Res. *88*, 4801–4810.

THURBER, C. H. (1981), *Earthquake Structure and Earthquake Locations in the Coyote Lake Area, Central California*, Ph.D. Thesis, Mass. Inst. of Technol., Cambridge, U.S.A.

THURBER, C. H. (1983), *Earthquake Locations and Three-dimensional Crustal Structure in the Coyote Lake Area, Central California*, J. Geophys. Res. *88*, 8226–8236.

TSELENTIS, G.-A., MELIS, N. S., and SOKOS, E. (1994), The Patras (July 14, 1993; $M_s = 5.4$) Earthquake Sequence, presented at the 7th Congress of the Geol. Soc. of Greece, Thessaloniki, May 25–27.

TSELENTIS, G.-A., XANALATOS, N., and MELIS, N. S. (1994), SISMWIN: A Computer Program for Seismological Dataphase Picking and Processing, Report C2, Patras Seismological Centre, 76 pp.

UNDERHILL, J. R. (1988), *Triassic Evaporites and Plio-Quaternary Diapirism in Western Greece*, J. Geol. Soc. London *145*, 269–282.

UNDERHILL, J. R. (1989), *Late Cenozoic Deformation of the Hellenide Foreland*, *Western Greece*, Bull. Geol. Soc. Am. *101*, 613–634.

(Received July 14, 1997, accepted December 12, 1997)